NANOSYSTEMS:
PHYSICS, CHEMISTRY, MATHEMATICS

Original article

Anannikov E.S., et al. *Nanosystems: Phys. Chem. Math.*, 2024, **15** (6), 806–813.
http://nanojournal.ifmo.ru
DOI 10.17586/2220-8054-2024-15-6-806-813

Synthesis and research of physical and chemical properties of $InGaZn_2O_5$ prepared by nitrate-glycolate gel decomposition method

Egor S. Anannikov[1], Timofey A. Markin[1], Ibrohimi A. Solizoda[1,2,4], Gleb M. Zirnik[1], Daniil A. Uchaev[3], Alexander S. Chernukha[1,2,3], Svetlana A. Gudkova[1,2], Denis A. Vinnik[1,2,3]

[1]Moscow Institute of Physics and Technology, Dolgoprudny, Russia

[2]St. Petersburg State University, St. Petersburg, Russia

[3]South Ural State University, Chelyabinsk, Russia

[4]Tajik National University, Dushanbe, Tajikistan

Corresponding author: Denis A. Vinnik, vinnik.da@mipt.ru

ABSTRACT Indium-gallium-zinc oxide $InGaZn_2O_5$ was synthesized by nitrate-glycolate gel decomposition method using ethylene glycol as a complexing and chelating agent. In this work, SEM, EDS and UV-vis-diffusion spectra of IGZO were obtained. $InGaZn_2O_5$ optical band gap was found using Kubelka–Munk transformation. The morphology of the particles was examined: at low sintering temperatures many micro-meter particles are observed, the sample is heterogeneous in crystalline state. At annealing temperatures above 800 °C a single-phase crystalline structure is observed.

KEYWORDS indium-gallium-zinc oxide, IGZO, $InGaZn_2O_5$, nitrate-glycolate gel, chelating reagent, ethylene glycol, chelate-nitrate method

ACKNOWLEDGEMENTS The research is supported by the Ministry of Science and Higher Education of the Russian Federation (state assignment) No. 075-03-2024-117, project number FSMG-2024-0028.

FOR CITATION Anannikov E.S., Markin T.A., Solizoda I.A., Zirnik G.M., Uchaev D.A., Chernukha A.S., Gudkova S.A., Vinnik D.A. Synthesis and research of physical and chemical properties of $InGaZn_2O_5$ prepared by nitrate-glycolate gel decomposition method. *Nanosystems: Phys. Chem. Math.*, 2024, **15** (6), 806–813.

1. Introduction

Research in electronics focuses on several areas. There are fields of semiconductor oxides research due to the potential for their usage in various devices such as memristors [1] and thin-film field-effect transistors (TFT) [2, 3]. TFT find the application in the production of modern displays and monitors [4–6]. At present, oxide semiconductor materials cannot completely replace silicon, but it is possible to use them as materials for flexible microelectronics, which is a new development direction for these materials. [7–9]. Among oxides, indium-gallium-zinc oxide (IGZO) is one of the most widely studied [10–13]. Amorphous indium-gallium-zinc oxide used for thin-film transistors (a-IGZO TFTs) have garnered significant interest due to their high electron mobility, straightforward fabrication process, cost-effectiveness, and excellent uniformity [11].

Additionally, IGZO exhibits great optical transparency and in order of magnitude, it can reaches higher than other materials on/off current ratio about 10^8 [10], which are advantageous for display technologies and optoelectronic applications. Its crystallinity also allows for uniform large-area deposition, enhancing scalability and enabling the development of high-resolution, energy-efficient electronic devices. The unique properties of IGZO make it highly suitable for applications in hybrid and microelectronic systems, where high-performance and stable materials are essential [4]. Its compatibility with flexible substrates and potential for integration into low-temperature processing make IGZO a promising candidate for next-generation electronic devices [5]. First, the single-crystal IGZO-based materials were investigated, later it was found that IGZO amorphous thin films also have great potentials for flexible electronics [13–15].

The first synthesized compound for TFT production was $InGaZn_5O_8$ [16], later, studies of IGZO with other concentrations began. Later, the most common studies were of the $InGaZnO_4$ composition (xIn:xGa:xZn = 1:1:1) [17–20]. Further works varied the ion ratio to study the whole concentration triangle [3, 17, 21, 22]. Despite this, the system has not been completely examined yet. For example, in [21], compositions with fixed stoichiometric ratio of Ga and Zn were studied and the amount of In was varied, while in [23], the amount of Ga was varied with fixed In and Zn [24, 25]. At the same time for the In–Ga–Zn–O system in the amorphous state, it is possible to vary the concentration of each element separately within a sufficiently wide range. Thus, by changing the concentration of an element, the properties of the device can also be changed. Unfortunately, this approach is well realizable for the amorphous IGZO only. In the crystalline state, the IGZO homogeneity area is strongly reduced (even at temperatures around 1350 °C [24, 25] and is limited to clearly defined chemical compositions $(In_{1-x}Ga_xO_3)_n(ZnO)_m$, where $x \neq 0$, $x \neq 1$, at strictly defined n and m.

In the process of using IGZO thin films in transistors, a large number of evaluation criteria have been obtained, including stability and degradation characteristics of these semiconductor devices [38–41]. Physical and chemical properties of IGZO such as charge carrier mobility, grain size, threshold voltage, and other characteristics directly depend on the method of synthesis and chemical composition of the final product. For example, increasing the content of In in the oxide increases the mobility of charge carriers [34, 35], and varying the amount of Ga leads to a change in the threshold voltage [22]. The synthesis conditions also affect the semiconductor properties. The annealing temperature affects the charge carriers concentration and mobility, the phase composition and sample morphology of the TFT [3, 18]. As shown in [36, 37], the electrical and optical properties of IGZO thin films depend on the degree of their crystallinity (or amorphous state).

One of the main research areas is the creation of thin semiconductor films. A lot of experimental material for obtaining the TFs and TFTs has been accumulated in [3,17–20,25–27]. Such methods as chemical/physical vapor deposition, pulsed laser deposition, molecular beam and epitaxy, atomic layer deposition, and magnetron sputtering are successfully applied to obtain IGZO-films. Recently, new methods of thin film synthesis, including spin-coating [28, 29] and microplotter-print [30, 31], have been improved. Advantages over classical methods include scalability and cheap implementation [3, 18, 32, 33].

As described above, IGZO has a huge potential for use in flexible electronics, including using the printing technologies. IGZO-based printing technology will allow one to expand the potential application area due to the use of thermally unstable, but extremely cheap and available plastic and paper substrates. To develop this concept, it is necessary to obtain extremely pure (X-ray clean) IGZO powders for their further use. In this case, there is few works devoted to $InGaZn_2O_5$ nanoparticles obtaining [42, 43]. Most often, they are obtained by the chelate-nitrate (sol-gel or self-combustion) method due to easy scaling and cheapness of the process. In our work, an oxide of $InGaZn_2O_5$ composition was obtained for the first time using ethylene glycol as a complexing agent; previously, it was prepared only with polyvinyl alcohol [44]. The dependence of the morphology of the samples on their sintering temperature was also investigated.

2. Methodology of experimental research

Nitrate-glycolate gel decomposition method was used for $InGaZn_2O_5$ synthesis according previous work [45]. Indium nitrate 4.5-aqueous [$In(NO_3)_3 \cdot 4.5H_2O$ ("c.p.")], gallium nitrate 9-aqueous [$Ga(NO_3)_3 \cdot 9H_2O$ ("c.p.")], zinc nitrate 6-aqueous [$Zn(NO_3)_2 \cdot 6H_2O$ ("c.p.")], and ethylene glycol ("p.a.") were used as reagent without further purification. All metal nitrates used in the synthesis were gravimetrically treated by calcination (800 °C, 12 h), so that the practical masses of nitrate-hydroxide salts were corrected according to the gravimetric data. The ratio of precursors was selected to obtain indium-gallium-zinc oxide with the ratio of In:Ga:Zn atoms = 1:1:2 in the product. The reagents were selected on a FA2204N balance. The solutions were stirred, heated, and evaporated in a magnetic stirrer with heating IKA® C-MAG HS7. Afterwards, the residual water in the gel was removed by holding it in a muffle furnace (Plavka.Pro PM-5 muffle furnace) in a ceramic cup. During the holding process, a self-combustion reaction occurred producing a solid substance. The solution after pouring into a ceramic cup was heated in the furnace from room temperature to 300 °C at a rate of 100 °C/hour, followed by isothermal holding for 6 hours. The samples were cooled to room temperature after passing through the self-combustion stage. Afterwards, the sample was divided into pieces and sintered in powdered form in alumina crucibles at temperatures from 400 to 1100 °C in 100 °C increments for 6 hours.

X-ray diffraction (XRD) was performed on a Drawell DW-XRD-2700A powder diffractometer (CuKα, 40 kV, 30 mA; $\lambda = 0.15406$ nm, Ni filter) in the range of 2θ angles from 5 to 95 ° at a rate of 5 ° per min at room temperature. Powder XRD pattern was used for lattice parameters calculation using the Jade 6.5 software package (Table 1).

The microstructure of samples was studied by scanning electron microscopy (SEM Jeol JSM-7001F, accelerating voltage 20 kV). In addition, the elemental composition was investigated and elemental distribution maps were drawn by EDX-spectroscopy (Oxford INCA X-max 80 EDS spectrometer, 20 kV electron beam energy). Due to the significantly higher energy value of the indium K-line compared to the K-lines of other elements in the studied samples, the indium content was calculated by the L-line, and for Zn, Ga and O by the K-line.

The crystal structure of the particles was studied by transmission electron microscopy (Jeol JSM-2100, accelerating voltage 160 kV). The morphology of the particles and their crystal structure state in the nanometer range were investigated.

Diffuse reflectance spectra were obtained for samples sintered at 500, 700, 900 and 1100 °C in the range from 250 to 800 nm at a recording rate of 1 nm/sec on a Shimadzu UV-2700 UV-Visible spectrophotometer. The background calibration was performed for pure barium sulfate $BaSO_4$ tablet. The sample was also applied to a barium sulfate tablet. The source of radiation in the near UV diapason was a deuterium lamp and in the near IR region was a tungsten filament halogen lamp. Switching between the light sources was done automatically when passing through the 320 nm wavelength. Diffuse reflection spectra were used to determine samples energy gap by the Kubelka–Munk transformation method. In Tauc-plot for the expression "$\alpha(h\nu)^n - h\nu$" n was equal to 2 for indirect allowed transitions.

3. Results and discussion

The XRD patterns of $InGaZn_2O_5$ samples annealed at different temperatures are presented in Fig. 1. The vertical red lines (dashed lines) show the allowed reflexes of $InGaZn_2O_5$ [46]. It was observed that at temperatures between 300 and 600 °C, broad maximums of the diffraction pattern are observed, which is responsible for the amorphous structure. In the range of 700 – 800 °C, the sample is in a weakly crystallized state. At annealing temperatures above 800 °C a single-phase crystalline structure is observed. No other reflexes (In_2O_3, ZnO etc.) were observed in the XRD patterns.

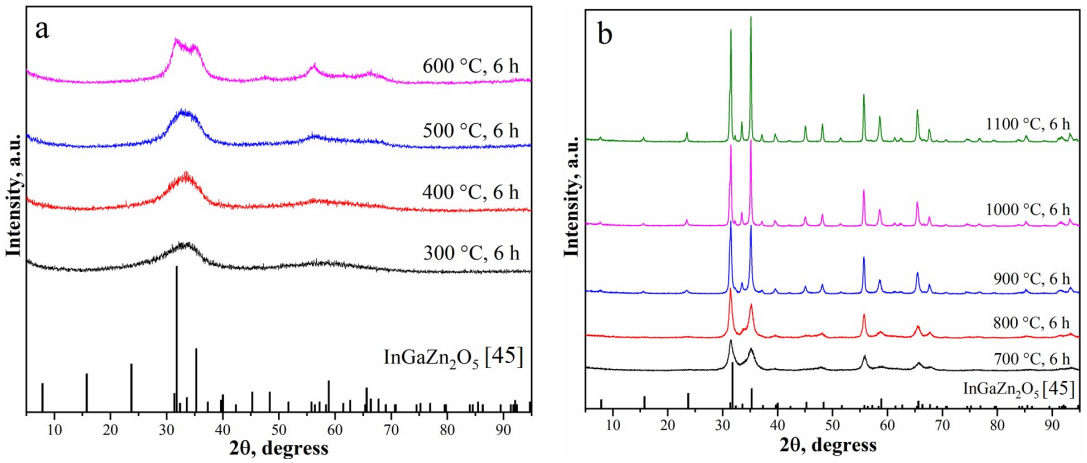

FIG. 1. XRD pattern of $InGaZn_2O_5$ samples annealing at 300 – 600 °C (a); 700 – 1100 °C (b). The dashed diagram shows the $InGaZn_2O_5$ phase [46]

The cell parameters were calculated only for the samples sintered at 700 – 1100 °C, the results are presented in Table 1. The given data are in correspondence with those obtained earlier [46].

TABLE 1. Calculated $InGaZn_2O_5$ lattice constants

No.	Sample	Unit cell parameters		
		***a*, Å**	***c*, Å**	**V, Å^3**
Sintering temperature, °C				
1	**700**	3.297±0.001	22.589±0.007	212.72±0.22
2	**800**	3.297±0.001	22.584±0.006	212.58±0.18
3	**900**	3.298±0.001	22.588±0.005	212.80±0.13
4	**1000**	3.298±0.001	22.591±0.005	212.84±0.12
5	**1100**	3.297±0.001	22.587±0.006	212.64±0.14
6	**[46]**	3.297±0.001	22.587±0.006	212.64±0.14

Figure 2 shows SEM images (in secondary electrons) of the $InGaZn_2O_5$ samples. Samples sintered at 500 and 700 °C (Fig. 2(a,b)) show many small particles with sizes 1 – 2 μm of abnormal shape. In Fig. 2(c,d), however, individual small particles become significantly smaller. As the annealing temperature increases, clearly faceted surface areas appear, which correlates with the XRD results, since the sample sintered at 1100 °C has a high degree of crystallization. At ×30000 zoom (Fig. 2(g,h)), it can be seen that the sample is an agglomerate of micro- and nanometer-sized crystallites.

The chemical composition of the samples was calculated using EDX-spectroscopy data. The distribution maps of the main elements are presented in Fig. 3. Their distribution is homogeneous throughout the sample for all temperatures of sintering (including 700 and 900 °C). This allows us to state the absence of amorphous regions of impurity phases and, thus, the presence of the sample in a single-phase state throughout the entire presented temperature range.

The chemical composition was calculated basis on the EDX-data. The relevant brutto formulas are presented in Table 2. The obtained data indicate the deviation from the specified composition within the error range (1 – 2 %).

Transmission electron microscopy (TEM) images are presented in Fig. 4. It shows $InGaZn_2O_5$ sample sintered at 500 °C. It can be seen that small particles are grouped together either in several pieces (Fig. 4a) or in large clusters (Fig. 4c). Large agglomerates of particles with different degrees of crystallization in sections are observed – both highly

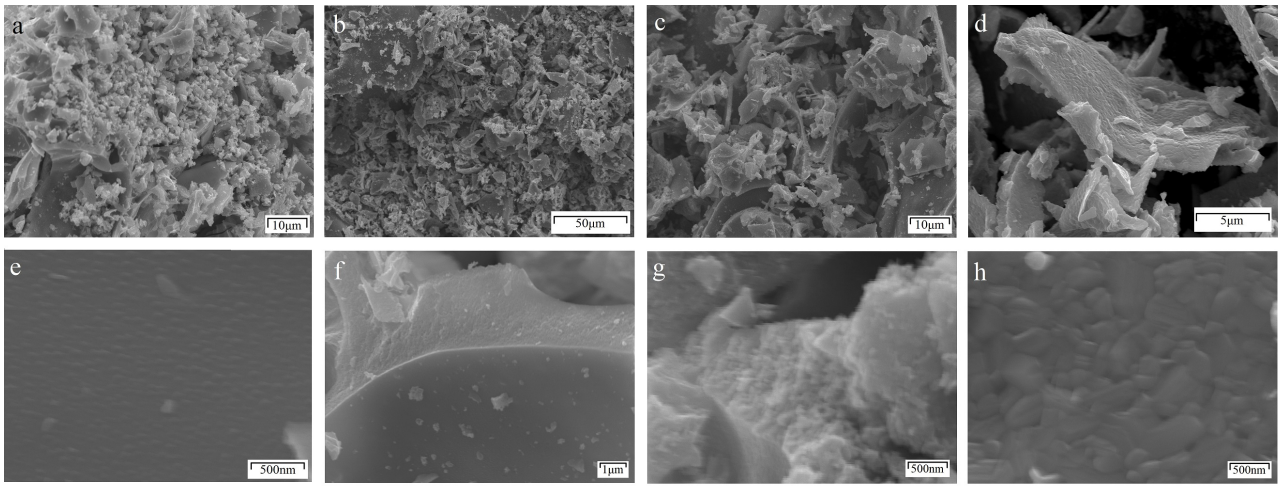

FIG. 2. SEM images of $InGaZn_2O_5$ samples sintered at 500 °C (a, e), 700 °C (b, f), 900 °C (c, g), 1100 °C (d, h) with various magnifications. The scale bar is indicated on the micrograph

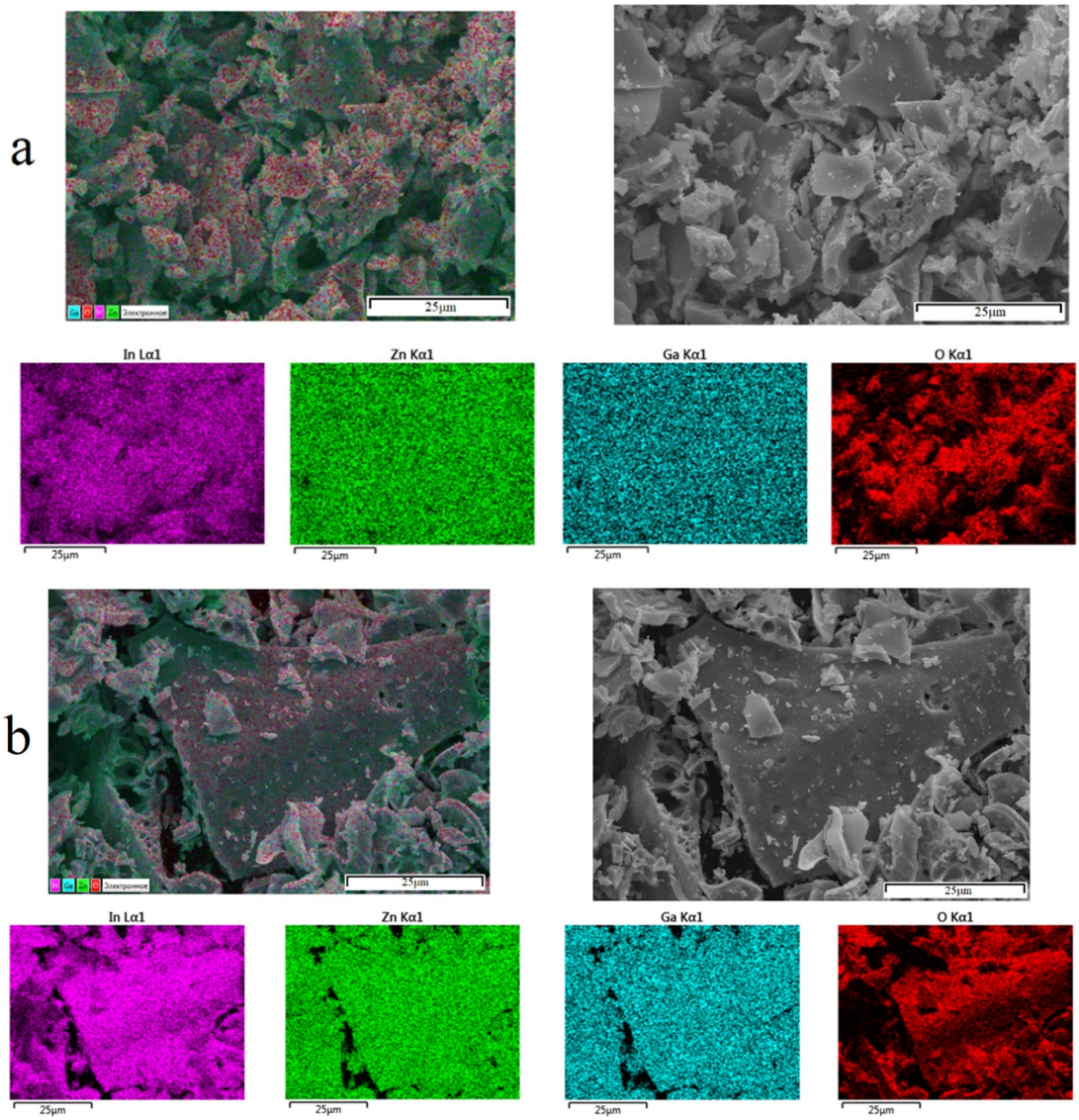

FIG. 3. SEM-images, multilayer EDX map and individual element map distribution (In – pink, Zn – green, Ga – blue, O – red) at sintering temperatures: a) 500 °C; b) 1100 °C. The scale bar is 25 μm for both samples

TABLE 2. Gross formula for $InGaZn_2O_5$ obtained at different temperatures

Annealing temperature	500 °C	700 °C	900 °C	1100 °C
Brutto formula	$In_{0.98}Ga_{0.98}Zn_{2.04}O_5$	$In_{1.02}Ga_{0.97}Zn_{2.01}O_5$	$In_{1.01}Ga_{0.97}Zn_{2.02}O_5$	$In_{1.00}Ga_{0.98}Zn_{2.02}O_5$

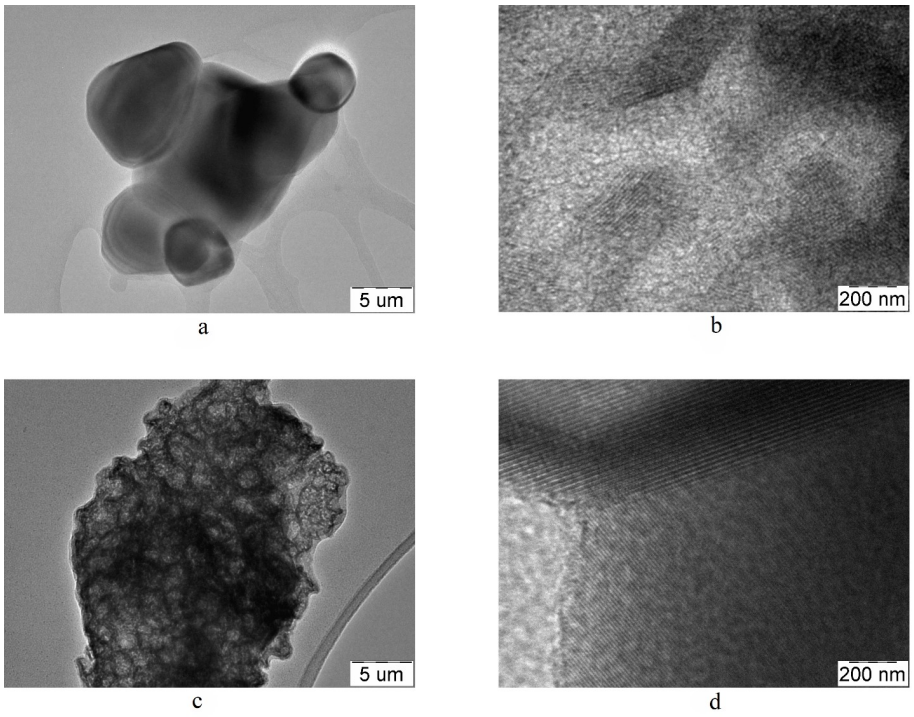

FIG. 4. TEM images of $InGaZn_2O_5$ samples at sintered temperature of 500 °C with different scale bar

crystallized (distinct bands in Fig. 4d) and low-crystallized (Fig. 4b). However, as can be seen, there is no way to calculate d-spacing because high resolution could not be achieved.

The UV-vis-spectroscopy results of the $InGaZn_2O_5$ samples are shown in Fig. 5. The sample does not have absorption peaks in the visible region. The band gaps calculation is given in Table 3, our results correlate with work published earlier [47]. $InGaZn_2O_5$ has a rather wide band gap, and it varies within the error during sintering in the temperature range from 500 to 1000 °C. This explains the fact that the band gap does not depend on the IGZO crystallinity and morphology.

TABLE 3. Band gap for $InGaZn_2O_5$ samples sintered at different temperatures

Annealing temperature, °C	500	700	900	1100	[47]
Band gap, eV	3.159	3.170	3.180	3.159	3.225

4. Conclusions

The nitrate-glycolate gel decomposition method was successfully applied to synthesize $InGaZn_2O_5$ samples. At temperatures from 300 to 600 °C an amorphous structure is observed, at 700 – 800 °C the sample is in a weakly crystallized state, and at annealing temperatures above 800 °C, a high crystalline structure is observed. The morphology of the samples is as follows: at low sintering temperatures many micro-meter particles are observed, the sample is heterogeneous in crystalline state. This is confirmed by TEM images. When the annealing temperature is increased, the particles are organized into clearly faceted structures. The bandgap width of IGZO is 3.17 eV, which correlates with literature data. The obtained data indicate that it is possible to obtain $InGaZn_2O_5$ using the nitrate-glycol method, which creates a scientific basis for using materials to obtain colloidal solutions (ink) and their use in printing technologies in the field of electronics.

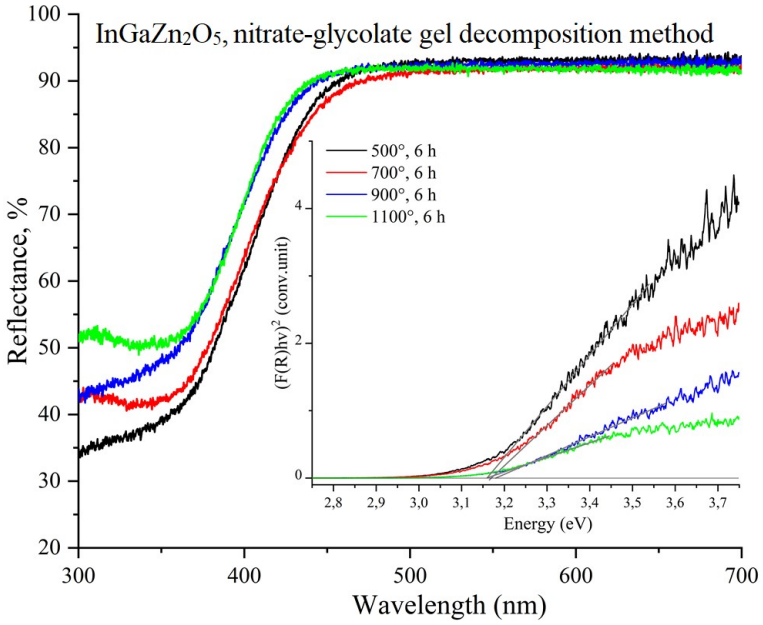

FIG. 5. UV-vis spectra of $InGaZn_2O_5$ for different sintering temperatures. Tauc-plot is presented in the inset

References

[1] Jang J.T., Min J., Hwang Y., Choi S.J., Kim D.M., Kim H., Kim D.H. Digital and Analog Switching Characteristics of InGaZnO Memristor Depending on Top Electrode Material for Neuromorphic System. *IEEE Access*, 2020, **8**, P. 192304–192311.

[2] Sporea R.A., Niang K.M., Flewitt A.J., Silva S.R.P. Novel Tunnel-Contact-Controlled IGZO Thin-Film Transistors with High Tolerance to Geometrical Variability. *J. Adv. Mater.*, 2019, **31** (36), 1902551.

[3] Olziersky A., Barquinha P., Vilà A., Magaña C., Fortunato E., Morante J.R., Martins R. Role of Ga_2O_3–In_2O_3–ZnO channel composition on the electrical performance of thin-film transistors. *Mater. Chem. Phys.*, 2011, **131** (1–2), P. 512–518.

[4] Kataoka Y., Imai H., Nakata Y., Daitoh T., Kimura T.M.N., Nakano T., Mizuno Y., Oketani T., Takahashi M., Tsubuku M., Miyake H., Hirakata T.I.Y, Koyama J., Yamazaki S., Koezuka J., Okazaki K. Development of IGZO-TFT and Creation of New Devices Using IGZO-TFT. *SID Symposium Digest of Technical Papers*, 2013, **44** (1), P. 771–774.

[5] Hendy I., Brewer J., Muir S. Development of High?Performance IGZO Backplanes for Displays. *Inf. Disp.*, 2022, **38** (5), P. 60–68.

[6] Hong T., Kim Y.S., Choi S.H., Lim J.H., Park J.S. Exploration of Chemical Composition of In–Ga–Zn–O System via PEALD Technique for Optimal Physical and Electrical Properties. *Adv. Electron. Mater.*, 2023, **9** (4), 2201208.

[7] Bhatti G., Agrawal Y., Palaparthy V., Mummaneni K., Agrawal M. Flexible Electronics: A Critical Review. In: Agrawal, Y., Mummaneni, K., Sathyakam, P.U. (eds) Interconnect Technologies for Integrated Circuits and Flexible Electronics. *Springer Tracts in Electrical and Electronics Engineering*, Singapore, 2024, P. 221–248.

[8] Bi S., Gao B., Han X., He Z., Metts J., Jiang C., Asare-Yeboah K. Recent progress in printing flexible electronics: A review. *Sci. China Technol. Sci.*, 2024, **67**, P. 2363–2386.

[9] Benwadih M., Coppard R., Bonrad K., Klyszcz A., Vuillaume D. High Mobility Flexible Amorphous IGZO Thin-Film Transistors with a Low Thermal Budget Ultra-Violet Pulsed Light Process. *ACS Appl. Mater. Interfaces*, 2016, **8** (50), P. 34513–34519.

[10] Xu X., He G., Wang L., Wang W., Jiang S., Fang Z. Optimization of electrical performance and stability of fully solution-driven α-InGaZnO thin-film transistors by graphene quantum dots. *J. Mater. Sci. Technol.*, 2023, **141**. P. 100–109.

[11] Xie Y., Cai K., Jian H., Huang Y., Weng J., Wang W. Study on Amorphous InGaZnO Thin-Film Transistor Modeling Method Based on Artificial Neural Network. *IEEE J. Electron Devices Soc.*, 2023, **11**, P. 717–725.

[12] Meléndrez Z.A.L., Durán A., Brown F., Negrete O.H., Paredes J.H., Montano V.E.A. Design of High-Entropy Ceramics with IGZO-Based Compounds for Electroceramics Applications. *Advances in Powder and Ceramic Materials Science 2023*, 2023, P. 3–10.

[13] Han Y., Lee D.H., Cho E.S., Kwon S.J., Yoo H. Argon and Oxygen Gas Flow Rate Dependency of Sputtering-Based Indium-Gallium-Zinc Oxide Thin-Film Transistors. *Micromachines*, 2023, **14** (7), P. 1394–1404.

[14] Lee Y.W., Choi S.H., Lee J.S., Kwon J.Y., Han M.K. Investigation of Amorphous IGZO TFT Employing Ti/Cu Source/Drain and SiNx Passivation. *MRS Online Proceedings Library*, 2011, **1321** (1906), P. 247–252.

[15] Lu Q., Huang X., Li F., Xin H., Huang H. Fabrication and Properties of Amorphous IGZO-TFT. *Proceedings of the 4th Workshop on Advanced Research and Technology in Industry (WARTIA 2018)*, 2018, **173**, P. 279–282.

[16] Nomura K., Ohta H., Ueda K., Kamiya T., Hirano M., Hosono H. Thin-Film Transistor Fabricated in Single-Crystalline Transparent Oxide Semiconductor. *Science*, 2003, **300** (5623), P. 1269–1272.

[17] Nomura K., Takagi A., Kamiya T., Ohta H., Hirano M., Hosono H. Amorphous Oxide Semiconductors for High-Performance Flexible Thin-Film Transistors. *Jpn. J. Appl. Phys.*, 2006, **45** (5B), P. 4303–4308.

[18] Xie Y., Wang D., Fong H.H. High-Performance Solution-Processed Amorphous InGaZnO Thin Film Transistors with a Metal–Organic Decomposition Method. *J. Nanomater.*, 2018, **2018** (1), P. 1–7.

[19] Liao P.-Y., Chang T.-C., Hsieh T.-Y., Tsai M.-Y., Chen B.-W., Tu Y.-H., Chu A.-K., Chou C.-H., Chang J.-F. Investigation of carrier transport behavior in amorphous indium–gallium–zinc oxide thin film transistors. *Jpn. J. Appl. Phys.*, 2015, **54** (9), 094101.

[20] Mohammadian N., Das B.C., Majewski L.A. Low-Voltage IGZO TFTs Using Solution-Deposited OTS-Modified Ta_2O_5 Dielectric. *IEEE Trans. Electron. Devices*, 2020, **67** (4), P. 1625–1631.

[21] Tari A., Lee C.-H., Wong W.S. Electrical dependence on the chemical composition of the gate dielectric in indium gallium zinc oxide thin-film transistors. *Appl. Phys. Lett.*, 2015, **107** (2), 023501.
[22] Lee D.-H., Park S.-M., Kim D.-K., Lim Y.-S., Yi M. Effects of Ga Composition Ratio and Annealing Temperature on the Electrical Characteristics of Solution-processed IGZO Thin-film Transistors. *JSTS*, 2014, **14** (2), P. 163–168.
[23] Nakamura M., Kimizuka N., Mohri T. The phase relations in the In_2O_3–Ga_2ZnO_4–ZnO system at 1350 °C. *J. Solid State Chem.*, 1991, **93** (2), P. 298–315.
[24] Yamazaki S., Kimizuka N. *Physics and Technology of Crystalline Oxide Semiconductor CAAC-IGZO: Fundamentals*. Wiley, New York, 2016. 310 p.
[25] Yang C.S., Huang S.J., Kao Y.C., Chen G.H., Chou W.-C. Physical properties of $InGaO_3(ZnO)$ with various content ratio grown by PAMBE. *J. Cryst. Growth*, 2015, **425**, P. 258–261.
[26] Lee J.-Y., Heo K.-J., Choi S.-G., Ryu H.G., Koh J.-H., Kim S.-J. Effects of Oxygen Injection Rates on a-IGZO Thin-film Transistors with Oxygen Plasma Treatment. *JSTS*, 2021, **21** (3), P. 189–198.
[27] Liu S.-J., Fang H.-W., Hsieh J.-H., Juang J.-Y. Physical properties of amorphous Mo-doped In–Ga–Zn–O films grown by magnetron co-sputtering technique. *Mater. Res. Bull.*, 2012, **47** (6), P. 1568–1571.
[28] Jo E., Ahn J.H., Ha T.E., Kim E., Im H., Kim Y.-S. A Study of Spin Coated a-IGZO TFT with Y-doped ZrO_2 Gate Insulators. *Proceedings of the International Display Workshops*, 2022, **29**, P. 354–357.
[29] Zalte M.B., Naik T.R., Alka A., Ravikanth M., Rao V.R., Baghini M.S. Passivation of Solution-Processed a-IGZO Thin-Film Transistor by Solution Processable Zinc Porphyrin Self-Assembled Monolayer. *IEEE Trans. Electron Devices*, 2021, **68** (11), P. 5920–5924.
[30] Yan X., Li B., Zhang Y., Wang Y., Wang C., Chi Y., Yang X. Effect of Channel Shape on Performance of Printed Indium Gallium Zinc Oxide Thin-Film Transistors. *Micromachines*, 2023, **14** (11), P. 2121.
[31] Zhang L., Guo Q., Tan Q., Fan Z., Xiong J. High Performance Amorphous IGZO Thin-Film Transistor Based on Alumina Ceramic. *IEEE Access*, 2019, **7**, P. 184312–184319.
[32] Chang J.S., Facchetti A.F., Reuss R. A Circuits and Systems Perspective of Organic/Printed Electronics: Review, Challenges, and Contemporary and Emerging Design Approaches. *IEEE J. Emerg. Sel. Top Circuits Syst.*, 2017, **7** (1), P. 7–26.
[33] Sanctis S., Hoffmann R.C., Bruns M., Schneider J.J. Direct Photopatterning of Solution–Processed Amorphous Indium Zinc Oxide and Zinc Tin Oxide Semiconductors – A Chimie Douce Molecular Precursor Approach to Thin Film Electronic Oxides. *Adv. Mater. Interfaces*, 2018, **5** (15), 1800324.
[34] Kimura M., Kamiya T., Nakanishi T., Nomura K., Hosono H. Intrinsic carrier mobility in amorphous In–Ga–Zn–O thin-film transistors determined by combined field-effect technique. *Appl. Phys. Lett.*, 2010, **96** (26), 262105.
[35] Kamiya T., Hosono H. Material characteristics and applications of transparent amorphous oxide semiconductors. *NPG Asia Mater.*, 2010, **2** (1), P. 15–22.
[36] Takagi A., Nomura K., Ohta H., Yanagi H., Kamiya T., Hirano M., Hosono H. Carrier transport and electronic structure in amorphous oxide semiconductor, a-$InGaZnO_4$. *Thin Solid Films*, 2005, **486**(1–2), P. 38–41.
[37] Nomura K., Kamiya T., Ohta H., Shimizu K., Hirano M., Hosono H. Relationship between non-localized tail states and carrier transport in amorphous oxide semiconductor, In–Ga–Zn–O. *Physica Status Solidi (A)*, 2008, **205** (8), P. 1910–1914.
[38] Chen T.-C., Chang T.-C., Hsieh T.-Y., Tsai C.-T., Chen S.-C., Lin C.-S., Hung M.-C., Tu C.-H., Chang J.-J., Chen P.-L. Light-induced instability of an InGaZnO thin film transistor with and without SiOx passivation layer formed by plasma-enhanced-chemical-vapor-deposition. *Appl. Phys. Lett.*, 2010, **97** (19), 192103.
[39] Hsieh T.-Y., Chang T.-C., Chen T.-C., Chen Y.-T., Tsai M.-Y., Chu A.-K., Chung Y.-C., Ting H.-C., Chen C.-Y. Self-Heating-Effect-Induced Degradation Behaviors in a-InGaZnO Thin-Film Transistors. *IEEE Electron Device Lett.*, 2013, **34** (1), P. 63–65.
[40] Hsieh T.-Y., Chang T.-C., Chen T.-C., Tsai M.-Y., Chen Y.-T., Jian F.-Y., Chung Y.-C., Tung H.-C., Chen C.-Y. Investigating the Drain-Bias-Induced Degradation Behavior Under Light Illumination for InGaZnO Thin-Film Transistors. *IEEE Electron Device Lett.*, 2012, **33** (7), P. 1000–1002.
[41] Chen T.-C., Chang T.-C., Hsieh T.-Y., Lu W.-S., Jian F.-Y., Tsai C.-T., Huang S.-Y., Lin C.-S. Investigating the degradation behavior caused by charge trapping effect under DC and AC gate-bias stress for InGaZnO thin film transistor. *Appl. Phys. Lett.*, 2011, **99** (2), 022104.
[42] Wu M.-C., Hsiao K.-C., Lu H.-C. Synthesis of $InGaZnO_4$ nanoparticles using low temperature multistep co-precipitation method. *Mater. Chem. Phys.*, 2015, **162**, P. 386–391.
[43] Fukuda N., Watanabe Y., Uemura S., Yoshida Y., Nakamura T., Ushijima H. In–Ga–Zn oxide nanoparticles acting as an oxide semiconductor material synthesized via a coprecipitation-based method. *J. Mater. Chem. C*, 2014, **2** (13), P. 2448–2454.
[44] Kondrat'eva O.N., Smirnova M.N., Nikiforova G.E., Razumov M.I., Khoroshilov A.V. Layered ceramics based on $InGaO_3(ZnO)_2$: Preparation and experimental investigation of high-temperature heat capacity and thermal conductivity. *J. Eur. Ceram. Soc.*, 2021, **41** (13), P. 6559–6566.
[45] Zirnik G.M., Chernukha A.S., Uchaev D.A., Solizoda I.A., Gudkova S.A., Nekorysnova N.S., Vinnik D.A. Phase formation of nanosized $InGaZnO_4$ obtained by the sol-gel method with different chelating agents. *Nanosystems: Phys. Chem. Math.*, 2024, **15** (4), P. 520–529.
[46] Kimizuka N., Mohri T., Matsui Y., Siratori K. Homologous compounds, $InFeO_3(ZnO)_m$ ($m = 1 - 9$). *J. Solid State Chem.*, 1988, **74** (1), P. 98–109.
[47] Préaud S., Byl C., Brisset F., Berardan D. SPS?assisted synthesis of $InGaO_3(ZnO)_m$ ceramics, and influence of m on the band gap and the thermal conductivity. *JACerS*, 2020, **103** (5), P. 3030–3038.

Submitted 9 October 2024; revised 12 November 2024; accepted 13 November 2024

Information about the authors:

Egor S. Anannikov – Moscow Institute of Physics and Technology, Institutsky lane, 9, Dolgoprudny, 141701, Russia; ORCID 0009-0003-2012-406X; anannikov.es@phystech.edu

Timofey A. Markin – Moscow Institute of Physics and Technology, Institutsky lane, 9, Dolgoprudny, 141701, Russia; ORCID 0009-0008-0598-1676; markin.ta@phystech.edu

Ibrohimi A. Solizoda – Moscow Institute of Physics and Technology, Institutsky lane, 9, Dolgoprudny, 141701, Russia; St. Petersburg State University, Universitetskaya embankment, 7–9, 199034, St. Petersburg, Russia; Tajik National University, Rudaki Av., 17, Dushanbe, 734025, Tajikistan; ORCID 0000-0001-6973-4633; solizoda.ia@mipt.ru

Gleb M. Zirnik – Moscow Institute of Physics and Technology, Institutsky lane, 9, Dolgoprudny, 141701, Russia; ORCID 0009-0008-4546-1368; glebanaz@mail.ru

Daniil A. Uchaev – South Ural State University, Lenin Av., 76, Chelyabinsk, 454080, Russia; ORCID 0000-0002-8623-4769; uchaevda@susu.ru

Alexander S. Chernukha – Moscow Institute of Physics and Technology, Institutsky lane, 9, Dolgoprudny, 141701, Russia; St. Petersburg State University, Universitetskaya embankment, 7–9, 199034, St. Petersburg, Russia; South Ural State University, Lenin Av., 76, Chelyabinsk, 454080, Russia; ORCID 0000-0002-1272-1628; chernukha.as@mipt.ru

Svetlana A. Gudkova – Moscow Institute of Physics and Technology, Institutsky lane, 9, Dolgoprudny, 141701, Russia; St. Petersburg State University, Universitetskaya embankment, 7–9, 199034, St. Petersburg, Russia; ORCID 0000-0002-3028-947X; svetlanagudkova@yandex.ru

Denis A. Vinnik – Moscow Institute of Physics and Technology, Institutsky lane, 9, Dolgoprudny, 141701, Russia; St. Petersburg State University, Universitetskaya embankment, 7–9, 199034, St. Petersburg, Russia; South Ural State University, Lenin Av., 76, Chelyabinsk, 454080, Russia; ORCID 0000-0002-5190-9834; vinnik.da@mipt.ru

Conflict of interest: the authors declare no conflict of interest.